Med Biol Eng Comput (2008) 46:1161–1167
DOI 10.1007/s11517-008-0384-1

SPECIAL ISSUE - ORIGINAL ARTICLE

Numerical flow simulation in the post-endoscopic sinus surgery nasal cavity

Guanxia Xiong · Jiemin Zhan · Kejun Zuo · Jianfeng Li · Liangwan Rong · Geng Xu

Received: 12 November 2007 / Accepted: 25 July 2008 / Published online: 26 August 2008

Abstract In this study we utilized computational fluid dynamic (CFD) techniques to construct a numerical simulation of nasal cavity airflow pre and post virtual functional endoscopic surgery (FESS). A healthy subject was selected, and CFD techniques were then applied to construct an anatomically and proportionally accurate three-dimensional nasal model based on nasal CT scans. A virtual FESS intervention was performed numerically on the normal nasal model using Fluent software. Navier-Stokes and continuity equations were used to calculate and compare airflow, velocity, distribution and pressure in both the pre and post FESS models. In the post-FESS model, there was an increase in airflow distribution in the maxillary, ethmoid and sphenoid sinuses, and a 13% increase through the area connecting the middle meatus and the surgically opened ethmoid. There was a gradual decrease in nasal resistance in the posterior ethmoid sinus region following FESS. These findings highlight the potential of this technique as a powerful preoperative assessment tool to aid clinical decision-making.

Keywords Functional endoscopic sinus surgery · Computational fluid dynamics · Laminar nasal airflow · Three dimensional reconstruction · Nasal cavity

G. Xiong · K. Zuo · G. Xu (✉)
Otolaryngology Hospital of the First Affiliated Hospital of Sun Yat-sen University, Otolaryngology Institute of Sun Yat-sen University, No. 58 Zhongshan Road 2, 510080 Guangzhou, People's Republic of China
e-mail: entxgfess@163.com

J. Zhan · J. Li · L. Rong
Department of Applied Mechanics and Engineering, Sun Yat-Sen University, 510080 Guangzhou, People's Republic of China

1 Introduction

Functional endoscopic sinus surgery (FESS) is commonly performed to relieve the symptoms of chronic rhinosinusitis. The operation involves initial uncinate and ethmoid excision, followed by opening of the maxillary, sphenoid and frontal sinuses. This procedure facilitates increased sinus ventilation and improved sinus draining through the opened middle meatus-anterior ethmoid complex (also known as the ostiomeatal complex). While FESS is generally highly effective in relieving the symptoms of chronic rhinosinusitis, there are some cases of reoccurrence and others where resolution is temporary. There are a number of possible explanations for FESS failure. These include local mucosal inflammation, inappropriate post-operative management, etc. FESS may also alter nasal cavity anatomy, leading to adverse changes in airflow and aerodynamics. Given this, it would be of significant clinical interest if pre-operative assessment could give an accurate indication of likely post-operative changes in nasal airflow. This would also allow for optimal surgical planning.

In the past, investigators have utilized models constructed from cadaver noses or amplified from CT and MRI images to study nasal flow [5, 7, 9, 14]. However such models tended to be inconvenient or inaccurate [5, 6]. More recently, with the advent of modern computational fluid dynamics (CFD) and advanced computer technology solutions for the Navier-Stokes equations that govern fluid flow dynamics within a complex conduit [2], transnasal aerodynamics can now be rapidly approximated using numerical simulations of various CT-generated three-dimensional (3-D) nasal models [9, 10, 12, 15]. Horschler and colleagues performed numerical flow simulations of nasopharyngeal airflow using CFD to determine sinus-site specific uptake of deleterious xenobacteria, pollutant

particulate deposition, airway obstruction, and olfactory capacity prior to surgical intervention [8]. A number of other more recent studies have utilized CFD in the analysis of nasal surgical intervention planning [10, 12, 15]. Indeed, Zhao et al. evaluated pre and post-surgical airflow with regards to odorant uptake using numerical modeling of an FESS-treated patient with chronic rhinosinusitis [18]. To our knowledge, however, the detailed turbulent effects and pressure–flow dynamics pre and post FESS are yet to be examined using CFD numerical simulations. Hence in this study we utilized 3-D reconstruction and CFD numerical flow to determine changes in nasal cavity airflow pre and post simulated FESS.

2 Materials and methods

The nomenclature of nasal anatomy used in this study is as described by Proctor [13].

2.1 Subjects

Thirty healthy adults in our research center were initially screened as possible subjects for 3-D nasal modeling. Seventeen of these individuals (ranging in age from 24 to 48 years) who had no histories of chronic or acute (within the preceding 3 months) nasal disease were further examined. Upon nasal endoscopic examination, 12 of these potential subjects were excluded due nasal septal deviation, hypertrophic or atrophic turbinates and/or superior, middle and inferior meatus abnormalities. Further assessment was carried out on the remaining five individuals using a noise acoustic rhinometer SRE 2000 (RhinoMetrics, Denmark). One potential subject exhibited a slightly abnormal air flow distribution and resistance curve and was subsequently excluded. Finally, CT scanning revealed that two of the remaining individuals had nearly normal nasal structure cavities. Of the two, a 40-year-old female was selected as the standard subject for this research. The other individual, a 26-year-old female, was excluded as she planned to become pregnant. The selected subject signed an informed consent form prior to taking part the study.

2.2 Three-dimensional nasal model reconstruction

The nasal cavity of the subject was scanned using a 64-slice high speed spiral CT (Toshiba, Nasu, Japan). Before scanning, the subject was required to rest at room temperature (approximately 24°C) for 30 min. Achieved images were taken as data source, slice thickness was 0.3 mm, and bone window was used. Horizontal CT image sections were analyzed using boundary extraction software (3D-Doctor, Able software Inc., Irvine, CA). The extracted boundary line of nasal cavity air flow was identified and modified by radiology and rhinology specialists. A series of coordinate output points were selected in the boundary line. Those points were taken as basic data for constructing a Fluent numerical model using Gambit software (6.1.22 edition of Fluent Company, Lebanon, PA). The model was constructed layer by layer, from inferior to superior, with a distance of 1.2 mm between each layer. The cavity model consisted of 112 layers and contained the complete nasal cavity area including all sinuses.

Based on the aforementioned simulated normal nasal cavity model, digitalized images of each nasal cavity layer were modified according to the FESS intervention. Post-operative data for each layer of the nasal cavity and sinus were simulated with respect to classical FESS, i.e., initial uncinate and then ethmoid sinus excision, followed by sinus opening of the maxillary, sphenoid and frontal sinuses. 3-D reconstruction was performed using Gambit software. The outline of the simulated classical nasal cavity model after simulated FESS was identical to that of the normal nasal cavity model. Each sinus opening area was decided upon according to standard functional endoscopic sinus surgery (the maxillary, sphenoid and frontal sinus openings were 1.0 cm × 0.8 cm, 0.6 cm × 0.5 cm and 0.4 cm × 0.4 cm, respectively).

2.3 Mesh generation

The models were constructed using tetrahedral mesh as previously outlined [17]. Mesh partitioning was dependent on different flow change in different areas. Layers were divided, and each mesh layer was divided further. The meshes were not identical. In narrower areas, mesh size was smaller. Therefore, the number of meshes in narrower areas could be compared to that in other areas. A total of 1,850,077 meshes were used in constructing this model (see Fig. 1a).

2.4 Boundary definition and conditions

The boundary definition and conditions were adapted from those described by Croce and colleagues [4]. The inferior part of nasopharynx was taken as the entry opening in both models. The flow rate at the opening was set at 353 ml/s. Considering the proximity of the anterior nostril to the nasal valve (the position of fastest flow field), the nostril was not taken as the end opening. The boundary was extended outside and a cylinder was added to the inferior part of anterior nostril. The two nostrils were connected and the boundary of the cylinder was taken as the end opening. The given pressure of the end opening was 1 atmospheric pressure ($P = 101\ 350$ Pa). Other nostril boundaries were solid walls. The nostril wall was assumed to be a rigid, no slip boundary.

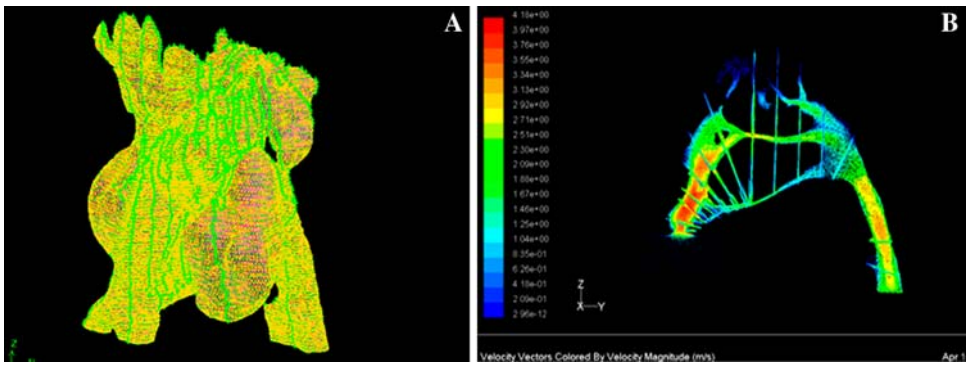

Fig. 1 Mesh generation and plane definition of the normal nasal cavity. **a** Mesh generation of the computational fluid model for the pre-functional endoscopic sinus surgery simulation. The nostrils are on the *lower left quadrant* and the nasopharynx on the *lower right quadrant*. **b** Eleven representative cross sections of selected sagittal planes for the pre-functional endoscopic sinus surgery. The nostrils are on the *left* and the nasopharynx on the *right*

2.5 Numerical simulation method

The Navier-Stokes equation of incompressible viscous fluid (laminar model) was employed to calculate the stable air flow during simulated inspiration [2].

2.6 Plane definition

Velocity vector was taken at cross section $X = 91$ mm. Along the direction of air flow (or velocity vector), the sections of plane 1–11 were vertical to $X = 91$ mm plane (also nearly vertical to the direction of velocity vector). Planes 1–11 encompassed the following: entrance of the anterior nostril; middle position of the nasal vestibule and nasal valve; anterior aspect of the inferior turbinate; anterior part of the middle turbinate; anterior aspect of the uncinate; middle part of the anterior ethmoid sinus; opening of the maxillary sinus; middle of ethmoid sinus; anterior wall of the sphenoid sinus; posterior nostril; middle area of the nasopharynx (Fig. 1b). The local flow field of the nasal cavity was calculated and analyzed by taking the areas thus mentioned as major points.

2.7 Calculation of airflow velocity and resistance of nasal cavity

Changes in mechanical resistance in the nasal cavity were represented by pressure decreases along the direction of air flow. Along with flow direction, above plane 1–11 were taken to measure left and right nasal cavity area in each plane and the downstream distance (downstream distance was the curve distance from anterior nostril along with sections mentioned above). Mean pressure in each section of the left and right nostrils was calculated and compared between each model to ascertain the difference in nasal cavity resistance.

3 Results

Pressure–flow magnitude changes at various selected planes from the entrance of the nose to the nasopharynx pre and post FESS are summarized in Table 1 and linearly depicted in Fig. 2. There was a gradual decrease in nasal resistance in the posterior ethmoid sinus region following FESS.

Figure 3 compares airflow distribution in the whole nasal cavity pre (a) and post (b) FESS. The simulated pressure change did not significantly alter airflow distribution or velocity (<0.01 m/s) in the pre-operative nasal model. In the post FESS model, however, there was an increase in airflow distribution (>0.01 m/s) in the maxillary, ethmoid and sphenoid sinuses. In the maxillary sinus of the post FESS model, upper airflow exceeded 0.1 m/s with an average velocity of 0.15 m/s and a peak velocity of 0.43 m/s. The anterior middle meatus average airflow was 1.07 m/s and the peak velocity was 1.07 m/s. The infundibulum, a narrow tubular passage that is connected superiorly and medially in the nasal cavity by the maxillary ostium, exhibited a velocity of less than 0.01 m/s. A high-velocity area formed at the anterior lower parts of the meatuses at $z = 66$ mm, with a central velocity reaching 3.3 m/s (Fig. 4). Vortices approaching 4.12 m/s were observed in the anterior inferior turbinate head, the vestibule and the nasal passages. The highest airflow was apparent along the nasal floor of the inferior meatus close to the septum, while the lowest airflow was through the superior region of the nasal cavity. Contour plots of airflow distribution for representative coronal cross-sections indicated annular airflow from the posterior of the maxillary sinus to the anterior of the maxillary sinus following FESS (Fig. 5).

Table 2 presents pre and post FESS airflow for the left and right nostrils in three specified regions (the inferior, middle, and superior meatuses). The total airflow rate of

Table 1 Pressure–flow magnitude over varying distances of selected planes in the nasal model pre-and post FESS

	Distance (cm)	Left nasal cavity		Right nasal cavity	
		Pre-operative	Post-operative	Pre-operative	Post-operative
Plane 1	0	−6.39	−6.43	−4.39	−4.37
Plane 2	0.5	−8.89	−8.91	−6.30	−6.27
Plane 3	1.1	−9.91	−9.96	−7.05	−7.05
Plane 4	1.54	−9.97	−10.05	−7.33	−7.38
Plane 5	2.24	−10.33	−10.52	−8.27	−8.39
Plane 6	2.91	−11.42	−11.58	−9.92	−10.02
Plane 7	3.75	−12.98	−13.13	−11.59	−11.72
Plane 8	5.37	−16.20	−15.16	−14.62	−13.57
Plane 9	6.42	−18.67	−16.86	−17.12	−15.22
Plane 10	7.52	−21.13	−19.68	−19.91	−18.37
Plane 11	8.54	−21.88	−20.57	−21.96	−20.61

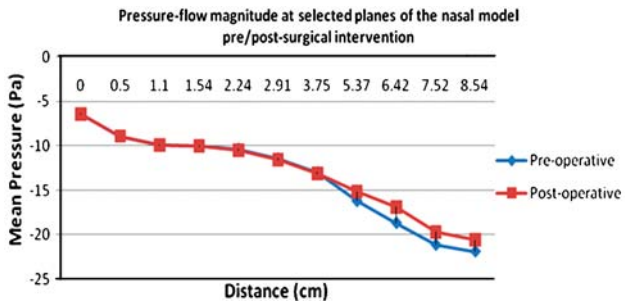

Fig. 2 Pressure–flow magnitude averaged over selected planes of the nasal model at various levels from the entrance of the nares to the nasopharynx pre- and post functional endoscopic sinus surgery

both nostrils (353 ml/s) before and after surgical intervention is in the middle range of flow rates for normal laminar breathing (200–500 ml/s) [17]. The left nostril flow rate (187.4 ml/s) was higher than that of the right (165.6 ml/s) as a consequence of nasal cycling (i.e., the total airway volume of the left nostril was greater than that of the right). This resulted in a higher airflow velocity (4.12 m/s) in the left nasal valve and inferior meatus region. In the post-FESS nasal cavity, airflow through the left and right nasal common meatuses decreased markedly, while flux through the area connecting the middle meatus and the surgically opened ethmoid sinuses increased by over 13%.

4 Discussion

In this study we utilized CFD and three-dimensional reconstruction techniques to assess basic changes in nasal cavity airflow following simulated FESS. This simulation revealed that FESS was associated with significant increases in airflow distribution and flux in the ostiomeatal complex and the paranasal sinuses. Given the lack of FESS efficacy in some cases, simulations such as reported herein may be useful for clinical planning in the future.

The results of our study are in general agreement with the aerodynamic distributions reported in other CFD numerically simulated nasal models in that the lowest airflow occurred through the superior region of the nasal

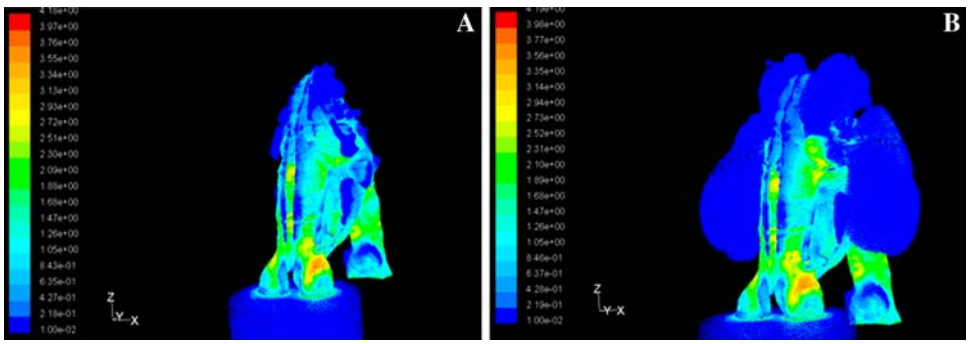

Fig. 3 Comparison of airflow distribution in the whole nasal cavity between pre-and post functional endoscopic surgery models. **a** Contour plot of velocity vector magnitudes from the normal nasal model indicating a lack paranasal sinus airflow (<0.01 m/s). **b** Velocity vector magnitude in the post functional endoscopic sinus surgery nasal model indicating a three-fold increase in airflow dynamics (>0.01 m/s) in the maxillary, ethmoid and sphenoid areas

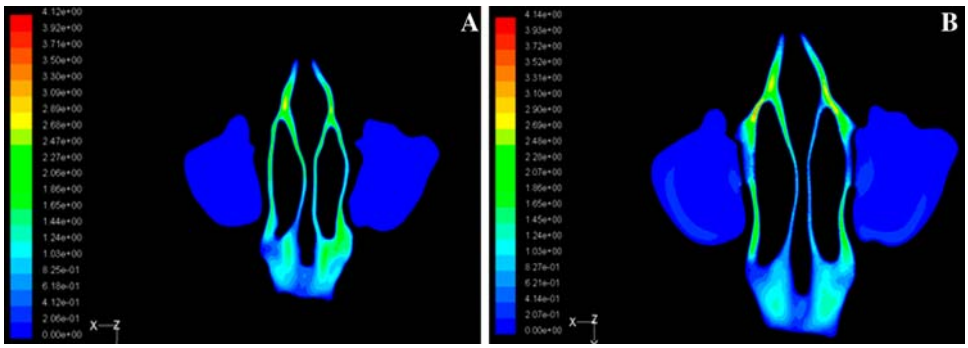

Fig. 4 Comparison of the velocity at cross section ($Z = 66$ mm) between the two models. The post functional endoscopic sinus surgery airflow velocity (**b**) was greater than that pre functional endoscopic sinus surgery (**a**)

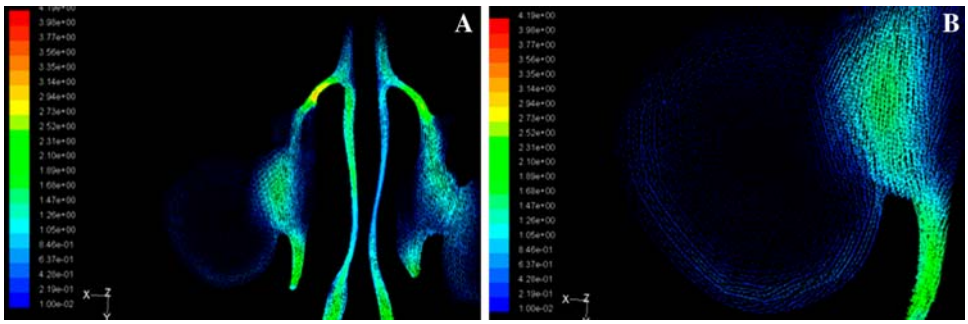

Fig. 5 Airflow distribution in the maxillary sinus post functional endoscopic sinus surgery. **a** and **b** show the maxillary sinus coronal cross-section depicting annular airflow from the posterior of the maxillary sinus to the anterior of the maxillary sinus

Table 2 A comparison of pre- and post functional endoscopic sinus surgery airflow in the left and right nostril

	Left Nostril ml/s (%)		Right nostril ml/s (%)	
	Pre-operative	Post-operative	Pre-operative	Post-operative
Common meatuses airflow	113.4 (60.5)	90.4 (48.2)	98.6 (59.5)	74.3 (44.9)
Inferior meatus airflow	20.5 (10.9)	18.6 (9.9)	27.5 (16.5)	25.4 (15.4)
Middle meatus airflow[a]	53.5 (28.6)	78.7 (41.9)	39.5 (24.0)	65.6 (39.7)
Global airflow	187.4 (100)	187.7 (100)	165.6 (100)	165.3 (100)

[a] Includes the ethmoid sinuses in the post-operative nasal model

cavity and the highest airflow occurred proximally along the nasal floor of the inferior meatus [17]. The global laminar inspiratory air-flow rate, however, was 353 ml/s, as compared to the general consensus of less than 250 ml/s [9, 15, 18]. Ecogeographic variations as a result of morphological adaptations to climate may explain this disparity. Tall, narrow ('leptorrhine') respiratory passages adapted to cold, dry climates manifest as a greater external nose protrusion and greater orientation of the conchae, implicating downwardly disposed nares that must negotiate a 90° bend from the external vestibule to the horizontal inner sinuses. This impedes inspiratory laminar flow. Anteriorly directed nares, such as those observed in short, broad (platyrrhines) respiratory passages facilitate laminar flow with less disruption, being more horizontal along the nasal floor [6]. Such morphological features are characteristic of the majority of the Asian populace, and are thought to facilitate a more energy efficient and undisrupted laminar inspiratory airflow [3]. To our knowledge this is the first investigation to use an Asian individual as a study model. This may explain the higher inspiratory flow rate.

Velocities and airflow distribution observed in this study are in close agreement to those reported in the literature. Vortices approaching 4.12 m/s were observed in the anterior inferior turbinate head, and high velocity areas formed in the anterior lower parts of the meatuses with a central velocity reaching 3.3 m/s in the pre-operative nasal model. Similarly, Subramanian et al. [15] and Keyhani et al. [10] reported values of 4.2 m/s in the posterior segment of the nasal valve at a flow rate of 250 and 4 m/s at the end of the nasal valve at a flow rate of 125 ml/s, respectively.

We observed a re-circulating airflow phenomenon in the posterior nasal valve and the lower parts of the meatuses following simulated FESS. This may be explained by sloping of the nasal roof, and nasal valve narrowing such that there is an abrupt acceleration when inspiratory air enters the vestibule, especially in the vertical planes of the nasal cavities. The vortex formation observed is most likely a consequence of high-pressure zones in the superior lateral portions of the nasopharynx, low pressure in the mid portions of the nasopharynx and an axial pressure gradient reverse to the main direction of flow [12, 18]. The resultant aerodynamic pressure–flow continuum is due to vertical

and lateral expansion of fused airways in the medial region and the dorsal and middle portions of the nasal cavity, and a significant lateral ventral segment narrowing.

The results of this study confirm that relatively minor anatomical changes may effectively alter airflow distribution [5]. In reality, more extensive anatomical alterations are frequently warranted for chronic rhinosinusitis patients who present with hypertrophied turbinates, septum deviations, nasal polyps, etc. Following FESS, dramatic changes in pressure flow and nasal aerodynamics are apparent in such individuals. Indeed, in a study employing CFD modeling, Zhao and colleagues demonstrated a >700% change in airflow through the olfactory region upon virtual resolution of artificial nasal obstruction. Nostril and nasal resistance remained unchanged.

Studies pertaining to CFD simulated endoscopic surgeries often neglect to take into account possible pre-existing anatomical/physiological conditions in the nasal passages that may influence inspiratory patterns. Physiological conditions such as perpetual congestion of one nostril, wet and warm nasal mucosal structures, combined turbulent and laminar airflow, and pathological anomalies attributed to chronic rhinosinusitis before FESS were neither assessed nor numerically simulated in this report. Hence, the precise validity of the findings pertaining to aerodynamics and pressure-flow and nasal resistance of FESS site-specific nasal structures could be considered somewhat compromised. Additional studies are warranted to examine how pre-virtual surgery variations in aerodynamics, turbulence, and odorant effects (as a consequence of morphological and pathological nasal anatomical abnormalities) influence nasal flow.

While the methodology for image based computational analysis of hemodynamics for preoperative surgical planning has been well established within the past decade [1, 11, 16], similar applications for use in the otorhinolaryngologic setting remain underdeveloped. Such applications necessitate sophisticated software to automatically handle medical images, segment structures of interest and create computational meshes for the extremely complicated subtle structures of the nasal cavity and paranasal sinus. Commercial software such as Mimics has been widely utilized for computational surgical simulation. However, in a preliminary trial using the most recent version of this program (v10, Materialise, Leuven, Belgium) we found that identification and resolution of subtle anatomical structures, such as the uncinate process and paranasal sinus ostia, was not satisfactory (data not shown). As the present investigation was our first numerical modeling simulation, we felt required to be extra cautious in guaranteeing the accuracy of the findings. Therefore the boundary conditions for the structures of nasal cavity and paranasal sinus were manually defined to ensure precise numerical reconstruction of the anatomical structures. This process was very time consuming and as such is not applicable for use in the clinical setting. One strategy to decrease this time would be to combine the automatic computational image handling and manual double-checks. While rough anatomical structures can be well identified by computer, manual interventions to define the fine structures would still be inevitable. This may reduce the workload to a more reasonable level for research applications, but would not be acceptable for routine clinical usage. Automation of the entire numerical reconstruction process would require further advances in resolution and power of both CT scanning and analytical software.

5 Conclusion

We have reported for the first time detailed turbulent effects and pressure–flow dynamics pre and post FESS using the techniques of numerical simulation and CFD. Our findings highlight the potential usefulness of CFD-generated numerical simulation as a powerful preoperative assessment tool to aid in clinical decision-making.

Acknowledgments This research was supported by grant number 5010 from the Clinical Medicine Research board of Sun Yat-Sen University.

References

1. Belleman RG, Sloot PMA (2001) Simulated vascular reconstruction in a virtual operating theatre. In: Lemke HU, Vannier MW, Inamura K, Farman AG, Doi K (eds) Computer assisted radiology and surgery (Excerpta Medica, International Congress Series1230). Elsevier, Berlin, pp 938–944
2. Cant S (2002) High-performance computing in computational fluid dynamics: progress and challenges. Philos Transact A Math Phys Eng Sci 360:1211–1225
3. Courtiss EH, Goldwyn RM (1983) The effects of nasal surgery on airflow. Plast Reconstr Surg 72:9–21
4. Croce C, Fodil R, Durand M et al (2006) In vitro experiments and numerical simulations of airflow in realistic nasal airway geometry. Ann Biomed Eng 34:997–1007. doi:10.1007/s10439-006-9094-8
5. Girardin M, Bilgen E, Arbour P (1983) Experimental study of velocity fields in a human nasal fossa by laser anemometry. Ann Otol Rhinol Laryngol 92:231–236
6. Hahn I, Scherer PW, Mozell MM (1993) Velocity profiles measured for airflow through a large-scale model of the human nasal cavity. J Appl Physiol 75:2273–2287
7. Hornung DE, Leopold DA, Youngentob SL et al (1987) Airflow patterns in a human nasal model. Arch Otolaryngol Head Neck Surg 113:169–172
8. Horschler I, Meinke M, Schroder W (2003) Numerical simulation of the flow field in a model of the nasal cavity. Comput Fluids 32:39–45. doi:10.1016/S0045-7930(01)00097-4
9. Keyhani K, Scherer PW, Mozell MM (1995) Numerical simulation of airflow in the human nasal cavity. J Biomech Eng 117:429–441. doi:10.1115/1.2794204

10. Keyhani K, Scherer PW, Mozell MM (1997) A numerical model of nasal odorant transport for the analysis of human olfaction. J Theor Biol 186:279–301. doi:10.1006/jtbi.1996.0347
11. Ku JP, Draney MT, Arko FR et al (2002) In vivo validation of numerical prediction of blood flow in arterial bypass grafts. Ann Biomed Eng 30:743–752. doi:10.1114/1.1496086
12. Martonen TB, Quan L, Zhang Z, Musante CJ (2002) Flow simulation in the human upper respiratory tract. Cell Biochem Biophys 37:27–36. doi:10.1385/CBB:37:1:27
13. Proctor DF (1982) The upper airway. In: Proctor DF, Anderson IB (eds) The nose: upper airway physiology and the atmospheric environment.Elsevier, New York, pp 23–42
14. Proetz AW (1952) Air currents in the upper respiratory tract and their clinical importance. Trans Am Laryngol Rhinol Otol Soc 53:73–103
15. Subramaniam RP, Richardson RB, Morgan KT, Kimbell JS (1999) Computational fluid dynamics simulations of inspiratory airflow in the human nose and nasopharynx. Inhal Toxicol 10:91–120. doi:10.1080/089583798197772
16. Taylor CA, Draney MT, Ku JP et al (1999) Predictive medicine: computational techniques in therapeutic decision-making. Comput Aided Surg 4:231–247
17. Wang K, Denney T, Morrison E, Vodyanoy V (2005) Numerical simulation of air flow in the human nasal cavity. Conf Proc IEEE Eng Med Biol Soc 6:5607–5610
18. Zhao K, Pribitkin EA, Cowart BJ, Rosen D, Scherer PW, Dalton P (2006) Numerical modeling of nasal obstruction and endoscopic surgical intervention: outcome to airflow and olfaction. Am J Rhinol 20:308–316. doi:10.2500/ajr.2006.20.2848